Characterisation of quantitative imaging biomarkers for inflammatory and fibrotic radiation-induced lung injuries using preclinical radiomics

Radiotherapy and Oncology 192 (2024) 110106

Contents lists available at ScienceDirect

Radiotherapy and Oncology

journal homepage: www.thegreenjournal.com

Original Article

Characterisation of quantitative imaging biomarkers for inflammatory and fibrotic radiation-induced lung injuries using preclinical radiomics

Kathryn H. Brown [a,*], Mihaela Ghita-Pettigrew [a], Brianna N. Kerr [a], Letitia Mohamed-Smith [a], Gerard M. Walls [a,b], Conor K. McGarry [b], Karl T. Butterworth [a]

[a] Patrick G. Johnston Centre for Cancer Research, Queen's University Belfast, Northern Ireland, UK
[b] Northern Ireland Cancer Centre, Belfast Health & Social Care Trust, Northern Ireland, UK

ARTICLE INFO

Keywords:
Radiomics
Preclinical models
Radiation pneumonitis
Pulmonary fibrosis
Imaging biomarkers
Prediction models

ABSTRACT

Background and purpose: Radiomics is a rapidly evolving area of research that uses medical images to develop prognostic and predictive imaging biomarkers. In this study, we aimed to identify radiomics features correlated with longitudinal biomarkers in preclinical models of acute inflammatory and late fibrotic phenotypes following irradiation.

Materials and methods: Female C3H/HeN and C57BL6 mice were irradiated with 20 Gy targeting the upper lobe of the right lung under cone-beam computed tomography (CBCT) image-guidance. Blood samples and lung tissue were collected at baseline, weeks 1, 10 & 30 to assess changes in serum cytokines and histological biomarkers. The right lung was segmented on longitudinal CBCT scans using ITK-SNAP. Unfiltered and filtered (wavelet) radiomics features (n = 842) were extracted using PyRadiomics. Longitudinal changes were assessed by delta analysis and principal component analysis (PCA) was used to remove redundancy and identify clustering. Prediction of acute (week 1) and late responses (weeks 20 & 30) was performed through deep learning using the Random Forest Classifier (RFC) model.

Results: Radiomics features were identified that correlated with inflammatory and fibrotic phenotypes. Predictive features for fibrosis were detected from PCA at 10 weeks yet overt tissue density was not detectable until 30 weeks. RFC prediction models trained on 5 features were created for inflammation (AUC 0.88), early-detection of fibrosis (AUC 0.79) and established fibrosis (AUC 0.96).

Conclusions: This study demonstrates the application of deep learning radiomics to establish predictive models of acute and late lung injury. This approach supports the wider application of radiomics as a non-invasive tool for detection of radiation-induced lung complications.

Introduction

Radiotherapy (RT) plays a critical role in the management of lung cancer particularly for small cell histology and unresectable non-small cell cases [1,2]. Despite advances in motion management, conformal deliveries, and dose estimation accuracy of contemporary RT techniques, normal tissue toxicities remain a significant cause of morbidity and mortality during survivorship [3–7]. Radiation-induced lung injury (RILI) has been reported in half of lung cancer patients treated with conventional RT, typically developing in the months-to-years after treatment [8,9].

Radiation pneumonitis (RP) is an early-phase, acute response driven by the infiltration of immune cells into the pulmonary interstitium and alveolar spaces, which can cause coughing, dyspnoea, and in more severe cases, hypoxia or death [10]. RP occurs in 15–40 % of patients with non-small cell lung cancer (NSCLC) treated with chemoradiation, which is moderate-to-severe in 10–20 % [9,11]. Pulmonary fibrosis (PF) is a late-phase, chronic toxicity caused by cumulative collagen deposition as permanent scars in the lung parenchyma, associated with progressive decrements in pulmonary function and increased rates of infection and hospitalisation [11,12]. The severity of RP and PF symptoms in terms of quality of life and mortality delegate these RILIs as primary safety endpoints in thoracic RT clinical trials [8,13–15].

Currently, the diagnosis of RILI is reliant on dosimetry and clinical assessments aided by CT density measurements. An increase in density of lung tissue on CT scans is typically an indicator of RILI. Yet, these tests

* Corresponding author at: Centre for Cancer Research, 97 Lisburn Road, Belfast BT9 7AE.
E-mail address: kathryn.brown@qub.ac.uk (K.H. Brown).

https://doi.org/10.1016/j.radonc.2024.110106
Received 25 September 2023; Received in revised form 10 January 2024; Accepted 17 January 2024
Available online 20 January 2024

are only capable of identifying damage when it is well established and are limited in accurately differentiating RP and PF [16–18]. The underlying mechanisms and risk factors for both pathologies remain only partially understood and therapeutic interventions are limited [19,20]. Importantly, no robust biomarkers of radiosensitivity are currently used in clinical practice to identify patients at highest risk of developing RILI [6,21,22].

Emerging studies have shown that quantitative image analysis (radiomics) in combination with patient factors can aid risk prediction for RP [22–26]. However, most of these studies have been performed retrospectively and do not correlate radiomics features with the underlying biological changes occurring during RP or PF [27,28].

Translatable preclinical models are essential for eliciting molecular mechanisms, the discovery of biomarkers and phase 0 testing of novel therapeutic interventions [29,30]. C3H/HeN mice harbour a spontaneous mutation at the lipopolysaccharide response locus resulting in an inflammatory-driven response to RT typical of RP [6,31–36]. C57BL6 mice are most commonly used in radiobiology studies due to similarities to human radiation response and in particular, PF in the lung [3]. In this study, these two strains were used as early and late RILI phenotypes for the interrogation of imaging with biological correlation, towards identification of radiomics signatures predictive of either RP or PF. We aimed to demonstrate the feasibility and advantage of using radiomics analysis to diagnose and differentiate RP and PF at early timepoints after irradiation and correlate longitudinal radiomics features with biological parameters.

Materials and methods

In vivo studies

All experimental procedures were carried out in accordance with the Home Office Guidance on the Operation of the Animals (Scientific Procedures) Act 1986 (PPL2935). Animal studies are reported in compliance with the ARRIVE guidelines [37].

Lung toxicity was investigated in female 8–10 weeks old C57BL/6J mice obtained from Envigo (n = 36) and female 8–10 weeks old C3H/HeN mice obtained from Janvier Laboratory (n = 36). All mice were housed under controlled conditions (12 h light–dark cycle, 21°C) in standard caging, and received a standard laboratory diet and water ad libitum. To improve the welfare of mice, environmental enrichment tools were placed in caging, such as cardboard tubes for exploration, and softwood blocks for gnawing and nesting material.

For each strain, mice were randomised into control (n = 18) or irradiated (n = 18) subgroups using an online random sequence generator. Lung tissues and blood samples were collected at baseline, and at 1, 10 and 30 weeks after irradiation. At baseline, 3 control mice per strain were culled and at weeks 1, 10 and 30, 5 control and 6 irradiated mice per strain were culled. Analysis was performed blinded for strain and treatment subgroups.

Prior to CBCT imaging and irradiation, animals were anaesthetised with ketamine and xylazine (100 mg/kg and 10 mg/kg) by intraperitoneal injection. Weights were monitored weekly, and all remained within our institutional weight loss tolerance of < 15 %.

Image acquisition and irradiation

Imaging and irradiation were performed using the Small Animal Radiation Research Platform (SARRP) (Xstrahl Life Sciences, Camberley UK), calibrated using the Institute of Physics and Engineering in Medicine and Biology (IPEMB) code of practice [38]. CBCT scans were acquired at 60 kV (0.5 mm Al filtration, 2.4 cGy). Image reconstruction was performed by Filtered Backprojection without postfiltering, log (white/x) was applied to input images using FDK with Hamming filtering window. CBCT scans were acquired immediately prior to irradiation and at weeks 1, 10, 20 and 30 post-irradiation. Lung injury was induced by delivering a single fraction of 20 Gy to the upper lobe of the right lung (dose rate 2.67 ± 0.11 Gy/min) using a 5 x 5 mm collimator with a parallel opposed beam arrangement (Supplementary Fig. 1).

CT tissue analysis

CBCT numbers were extracted from the irradiated section of the right lung from longitudinal CBCT scans. These were used as an indicator of tissue density and presence of fibrotic tissue (higher values indicative of higher density). Significance testing of differences between time points was conducted using 2-way AVOVA and is reported as $^{**}p < 0.01$, *** 0.0001, **** <0.0001.

Analysis of serum cytokines and bioinformatics analysis

Mouse XL Proteosome Profiler Cytokine arrays (ARY028, R&D Systems, UK) were performed to simultaneously characterise the expression of 111 cytokine targets. Each cytokine was sampled in duplicate on the membrane. Serum used for analysis was isolated from blood samples at week 1, 10 and 30. Cytokine arrays were performed according to the manufacturer's instructions using pooled serum samples for each treatment group (5 control and 6 irradiated mice per strain). Membranes were visualised using the GBox Imager and Syngene software. Quantification of signal intensities was performed with GeneTools software and densitometry values for spots on irradiated membranes were normalised to that of age-matched controls. Cytokine arrays were completed in one independent experiment. Proteins which satisfied a threshold of > 2- and < 0.5-fold change were considered differentially expressed and selected proteins were transformed into their corresponding gene names. Additional analysis was performed using the online gene set enrichment analysis tool, Enrichr [39].

Histological analysis

Lung tissues were harvested at baseline and weeks 1, 10 and 30 post-irradiation (5 control and 6 irradiated mice per strain). Lungs were inflated with PBS, fixed with 4 % formaldehyde, processed for histological evaluation, paraffin embedded and cut into 5 mm sections for staining. All slides were warmed to 60°C and subjected to a series of deparaffinization and rehydration steps. Slides were stained with Masson's Trichrome (AB150686, Abcam, UK) according to the manufacturer's instructions. Stained slides were scanned at X20 using the Leica AT2 Aperio (Brightfield scanner) for analysis and 5 random sections from the upper lobe of the right lung were used from each slide for analysis. Fibrosis was quantified from collagen deposition detected by the positive blue staining in lung samples at baseline and 1, 10 and 30 weeks after irradiation. Quantification of collagen deposition at these timepoints was compared to that found in 5 random sections of the right lung of age-matched control (unirradiated) mice. Slides were manually inspected and those which included air bubbles or artefacts from staining were excluded. An inhouse Matlab 2017a code was used to cluster the histologic images and then extract the blue fraction from each image [34]. Age dependent changes in fibrosis are presented in Supplementary Fig. 2. Significance testing of differences between time points was conducted using 2-way AVOVA and is reported as *<0.05, ** < 0.01, *** 0.0001.

Lung segmentation

Using CBCT imaging acquired on the SARRP, the whole right lung of all mice was auto-segmented for feature extraction [40]. Lung segmentations were created using the "semi-automatic active segmentation" tool in ITK-SNAP software (version 3.8.0, http://www.itksnap.org). Thresholding was used to differentiate the lungs to other surrounding structures (6,890 – 11,200) and manually altered where required.

Radiomics analysis

Handcrafted radiomics features were extracted from lung segmentations from CBCT scans using PyRadiomics software (version 2.7.7) [41], with a resampled PixelSpacing of 0.26 mm (the same as at image acquisition) and a fixed bin width of 25 [42]. Both unfiltered and filtered (wavelet) features were extracted for analysis. A total of 842 features were extracted and classified by the following feature classes: morphology (shape), intensity (first order) and texture (gray level co-occurrence matrix (GLCM), gray level run length matrix (GLRLM), gray level size zone matrix (GLSZM), gray level dependence matrix (GLDM) and neighbouring gray tone difference matrix (NGTDM) [41,43].

Delta radiomics features were calculated as outlined below:

$$Relative\ net\ change = (feature[end] - feature[start])/feature[start]$$

Principal component analysis (PCA) was performed on radiomics and delta radiomics datasets for the right lung using the *prcomp* package in RStudio software (version 4.1.2). Data was centered, scaled to unit variance ("GramSchmidt") and principal components (PC) computed using the singular value decomposition (SVD) method. Results from PCA's were visualized with PC1 and PC2 scores plotted on the x-axis and y-axis respectively and ellipses added (*stat_ellipse* function). Polygon ellipses were added assuming normal distribution with a confidence level of 0.95. PCA was used to compare changes over time in irradiated lung for each strain compared to baseline and comparison of inter-strain delta features. Radiomics features which were highly correlated to PC1 or PC2 were identified using Pearson's correlation (<0.8 or > -0.8). Significance testing of differences between time points was conducted using 2-way AVOVA and strain differences at each timepoint was assessed using unpaired t-tests.

Deep learning was performed using the open-source Precision-medicine-toolbox to identify predictive features for early and late injury [44]. Outcome prediction parameters were based on non-irradiated (control) and irradiated (RILI) groups. Scans from 1-week after irradiation were used for prediction of early damage (inflammation/RP) and scans from 20 and 30 weeks were combined and used for prediction of late damage (PF). Prediction models were created using a Random Forest Classifier (RFC). Scans were split into training (70 %) and validation (30 %) cohorts. For each mouse strain, 5 features were selected using recursive feature elimination (RFE) [45]. The RFC model was used for prediction of early (week 1) and late effects (weeks 20 & 30) in both mouse strains.

Results

CBCT numbers were extracted from longitudinal scans as a non-invasive imaging marker of fibrosis in the lung (Fig. 1). Radiological lung tissue density was indicative of fibrosis in the right lung of both mouse strains from the irradiated areas at 30 weeks ($p < 0.001$, Fig. 3B). However, there was not a significant increase in tissue density at earlier timepoints of 10 or 20 weeks ($p = 0.1579$–0.999).

Blood samples obtained at 1, 10, and 30-weeks after irradiation were used for cytokine analysis (Supplementary Table 1). The observed changes in cytokine levels are grouped according to inflammatory or fibrotic functions (Fig. 2A). At 1 week after irradiation, we observed the significant upregulation of pro-fibrotic cytokines in C57BL6 mice including CCL2 (2.04-fold) recruiter of pro-fibrotic monocytes, M−CSF (1.90-fold) facilitator of the first stages of fibroblast recruitment and PAI-1 (2.32-fold) linked to deposition of extracellular matrix in damaged tissue [6]. These mice also showed a significant early upregulation of inflammatory pathways at different timepoints, for example, IL-6 (18.7)

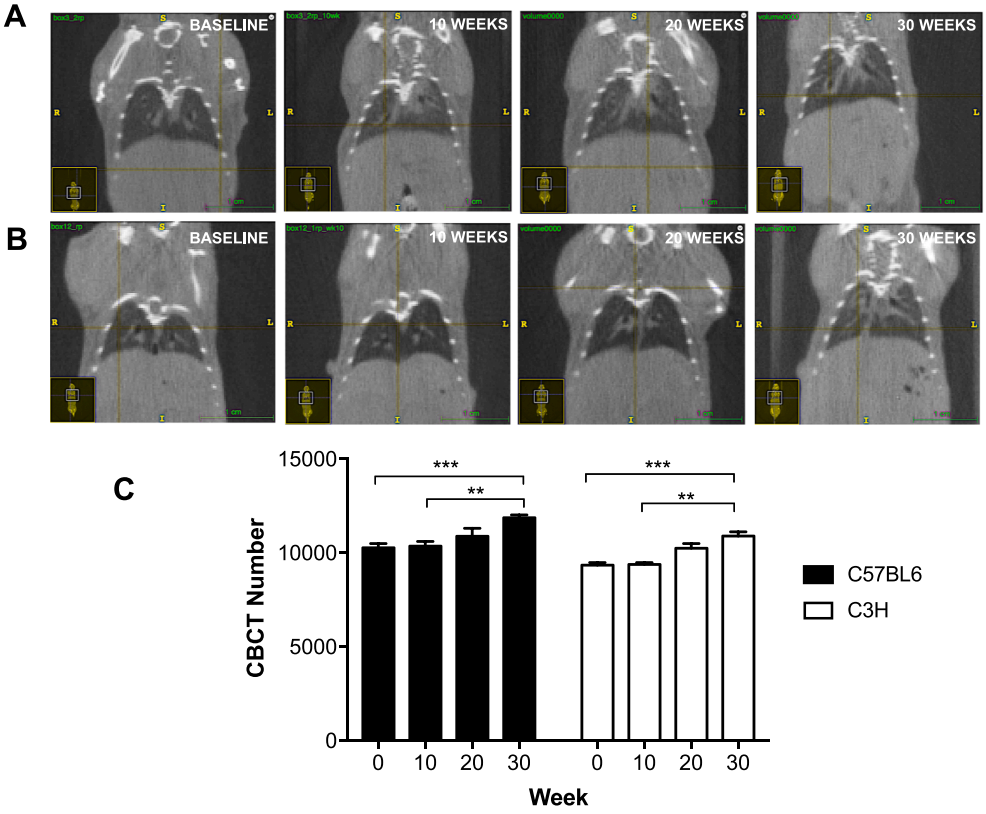

Fig. 1. CBCT scans acquired on the Small Animal Radiation Research Platform. Representative longitudinal scans for a single mouse acquired at baseline, 10, 20 and 30 weeks post irradiation for C57BL6 (Panel A) and C3H (Panel B) mice. Panel C: CBCT values extracted from irradiated areas of the right lung as an indicator of increased lung density due to fibrotic tissue. CBCT data presented as an average for 6 mice per strain at each timepoint ± standard error of the mean. Significance values are classified as ** < 0.01, *** 0.0001.

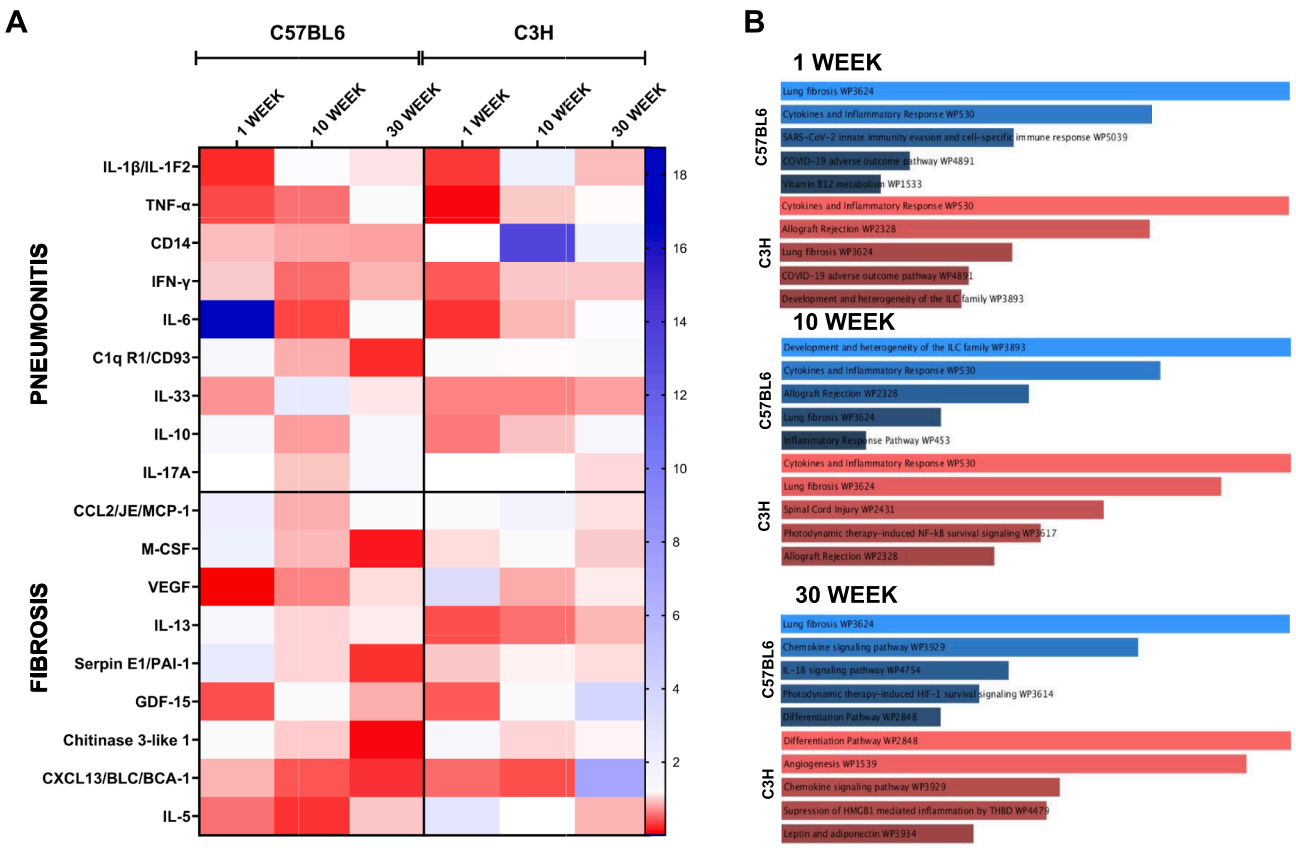

Fig. 2. Longitudinal variations in serum cytokines after irradiation and pathway enrichment analysis in C57BL6 and C3H/HeN. Panel A: A heatmap to represent the fold-change in cytokine expression for the two mouse strains at 1, 10 and 30 weeks post irradiation compared to age matched controls (data is grouped for 5 control and 6 irradiated mice per timepoint). Cytokines have been grouped into those associated with pneumonitis or fibrosis. Panel B: Gene enrichment outputs from Enrichr. Cytokines with a threshold of > 2- and < 0.5-fold change were considered differentially expressed and included in analysis.

at 1 week and IL-33 (2.25) at 10 weeks. IL-6 has both pro- and anti-inflammatory roles in responses to lung injury and has been strongly associated with chronic inflammation and hyper-profibrotic phenotypes [14,46,47].

In contrast, markers of acute lung inflammation and neutrophil influx were detected in C3H mice from weeks 1 to 10 after irradiation through increased expression of CD14 (13.5-fold), VEGF (3.6-fold) and IL-1β (1.86-fold) [35,48]. Interestingly, the anti-inflammatory cytokine, IL-10, was also downregulated at 1- and 10-weeks after irradiation in C3H mice. IFN-γ was downregulated in both strains throughout the study. At 30-weeks, C3H mice showed a 6.93-fold upregulation of CXCL13 which is a known prognostic marker of idiopathic pulmonary fibrosis [49]. The fibroblast activator GDF-15 was also upregulated (3.76) at 30-weeks. This suggests that although C3H mice are characteristically representative of RP they may have the potential to exhibit a PF phenotype.

Pathway enrichment analysis determined from cytokine expressions that the C57BL6 irradiated cohort was indicative of PF from as early as 1-week and the C3H irradiated cohort was prone to RP with fibrotic markers present from 10-weeks (Fig. 2B).

Masson's trichrome staining of irradiated lung tissue is shown in Fig. 3. Quantitative analysis of blue-positive staining showed no significant changes in collagen levels in the lungs of C3H mice compared to baseline controls ($p > 0.3761$). However, a significant increase in collagen deposition was observed in the lungs of C57BL6 mice from as early as 1 week, with a peak change at 30-weeks post-irradiation.

Radiomics features were extracted from longitudinal CBCT scans for quantitative image analysis (Fig. 1A & B). Principal component analysis (PCA) was used to identify radiomics features which correspond to biological trends (Fig. 4, Supplementary Fig. 3). Cytokine and tissue analysis confirmed that the C57BL6 strain had a fibrotic phenotype which developed over the 30-week study. The progressive fibrosis was correlated with the inverse correlation (descending shift) of PC2 (12 features) (Fig. 4A). This was statistically significant at 10- ($p = 0.0155$), 20- ($p = 0.0003$) and 30-weeks ($p < 0.0001$) after irradiation.

C3H mice had a prolonged inflammatory response (to 20 weeks) after irradiation supported by the high degree of overlap and correlation of the subgroups shown in Fig. 4B. Biological data indicated that C3H mice developed a later fibrotic phenotype identified by the inverse correlation (left shift) of PC1 for the 30-week subgroup (181 features) ($p = 0.0282$) (Fig. 4B).

Delta radiomics analysis (relative net change) differentiated the mouse strains at each imaging timepoint (Fig. 4C). Features related to these principal components are indicative of the biological differences seen in cytokine expression and histology at these respective timepoints. At 1 week after irradiation there was a high correlation in the strains indicative of the early inflammatory response seen in both. There was a significant difference in PCA clusters at 10- ($p = 0.0134$) and 20-weeks ($p = 0.0132$) after irradiation associated with PC1 when only the C57BL6 mice presented with fibrosis. A greater overlap in delta radiomics features at 30 weeks ($p = 0.0778$) may be due to the later onset of fibrosis in C3H mice identified by markers of fibroblast activation (GDF-15 and CXCL13) and histological changes.

RFC prediction models are shown in Fig. 5 to determine the radiomics features found to be most relevant for differentiating control and irradiated cohorts at early (1-week) and late (20–30 weeks) timepoints. Five radiomics features were identified for each model construction through RFE methods. From analysis of the 1-week scans in C3H mice radiomics features had a strong predictive power (AUC 0.88, Fig. 5C) related to inflammatory response. The most accurate predictive power

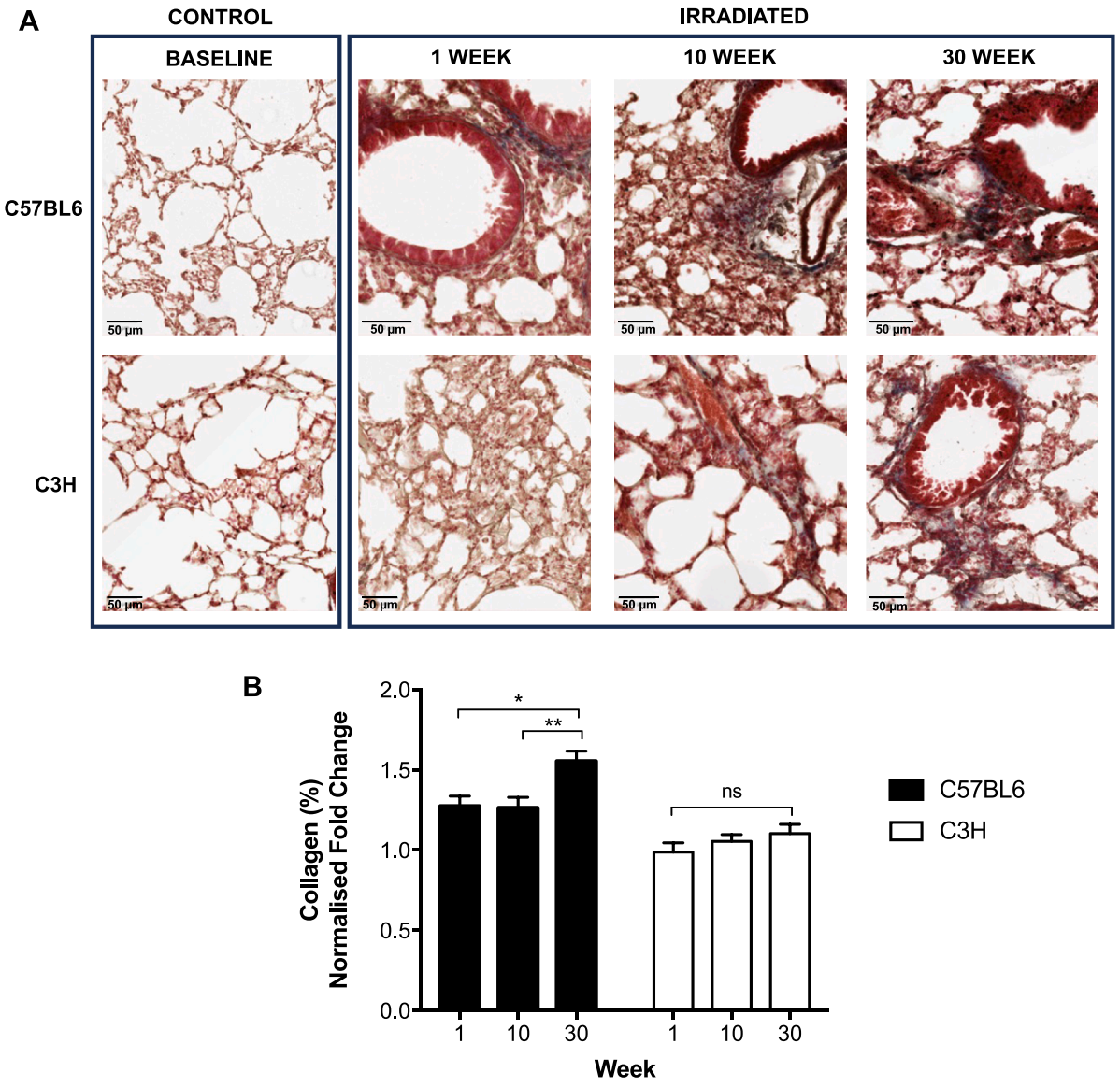

Fig. 3. Fibrosis staining of lung tissue for control and irradiated C57BL6 and C3H mice. Panel A: Lung tissue was harvested at baseline and weeks 1, 10 and 30 post irradiation and stained with Masson's Trichrome to identify collagen deposition. Fibrotic tissue can be identified from the blue staining of collagen fibres. Panel B: Fold-change of fibrotic deposition in lung tissue samples through quantification of blue pixels in samples in comparison to baseline control slides. Histology slides from 3 to 5 mice (control) or 4–6 mice (irradiated) were used for analysis with significance values of $*p = 0.0125$ and $**p = 0.0025$. (For interpretation of the references to colour in this figure legend, the reader is referred to the web version of this article.)

for fibrosis in the lung was identified in C57BL6 mice (AUC 0.96, Fig. 5D). From biological data, early markers of fibrosis are present in C3H mice at 30 weeks after irradiation, from imaging data, a strong predictive model for early detection was created (AUC 0.79, Fig. 5E). These results show that radiomics analysis is a reliable method to detect RILI and provides a promising outlook for the development of imaging biomarkers for early (RP) and late (PF) disease.

Discussion

This study aimed to characterise responses to RILI in two established mouse models that manifest differential phenotypes associated with RP (C3H) and PF (C57BL6) and to identify radiomics features predictive of the biological characteristics of these models. C3H mice are prone to RP and were selected to model early radiation effects. C57BL6 mice model late radiation effects due to their propensity for developing RT-related PF, similar to that of humans [6,36].

CT-based imaging is routinely used for treatment planning, to assess disease burden, and follow-up analysis in lung cancer patients receiving RT [18,50]. Identification of RILI from interval post-treatment scans could aid early detection in the selection of patients for intensive follow-up and referral to respiratory specialists, in order to minimise morbidity and prevent treatment-related death [51]. Previous studies have used grading based on clinical assessment and radiographic findings as an indicator of RILI [16,17,52–55], with an increase in regions of radio-opacity (high density) typically associated with an increased dose-dependency and over time [34,56–59], but these studies have not included radiomics analysis. Expert radiologists are required to score and identify glass opacites, reticular patterns and airspace consolidations leading to subjectivity in results in differentiating RP to local recurrence or fibrosis [54]. Density measurements have also been used to build and train RILI classifiers to automatically label damaged tissue [18]. In this study, CBCT density was only an indicator of fibrosis when it was well established at 30-weeks after irradiation.

Other studies have used Hounsfield units (HU) for the detection of air space enlargement and thus structural changes after lung irradiation in

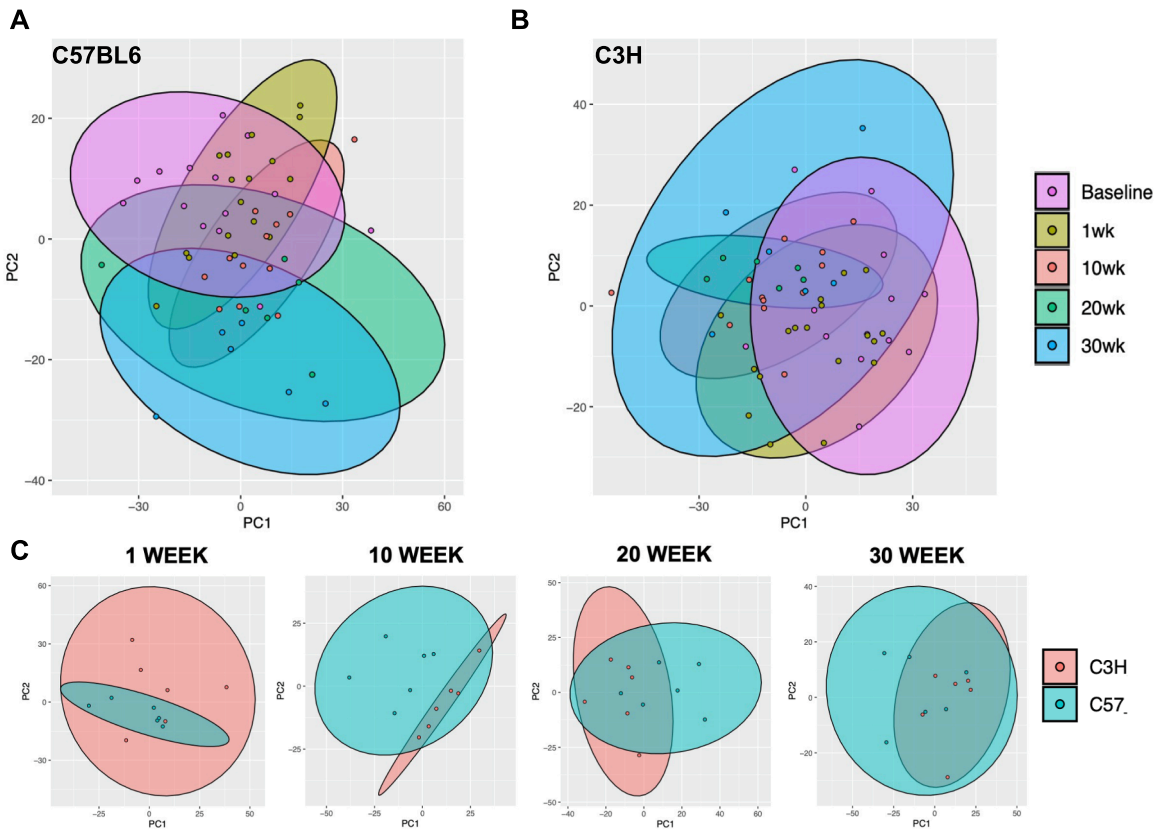

Fig. 4. Principal component analysis (PCA) plots of handcrafted radiomics features extracted from the right lung of C57BL6 and C3H cohorts from baseline to 30 weeks. Single points represent one experimental unit (n = 6–18) and ellipses represent the clustering of each timepoint. Panel A: PCA clustering of C57BL6 mice from baseline (pink) to 1 week (yellow), 10 weeks (red), 20 weeks (green) and 30 weeks (blue). Indicative of the progression towards a fibrotic phenotype associated with features related to PC2. Panel B: PCA clusters for C3H mice from baseline (pink) to 1 week (yellow), 10 weeks (red), 20 weeks (green) and 30 weeks (blue). A high overlap of PCA clusters in C3H mice is due to immune-mediated phenotype. Panel C: Delta radiomics features for C3H (red) and C57BL6 (blue) irradiated mice were compared at each imaging timepoint between the two mouse strains. Additional data associated with PCA including PCA scores and features are included in Supplementary Files 4–6. (For interpretation of the references to colour in this figure legend, the reader is referred to the web version of this article.)

mouse models [60]. Although this study reports the capabilities of detecting damage in the lung from micro-CT scans 1–4 days after irradiation it does not correlate HU values to damage developing weeks to months after irradiation, more associated with RP and PF. MRI scans are the most effective at detecting inflammatory effects in soft tissues excluding the lungs due to respiratory motion which causes imaging artefacts [61], yet they can provide information on pleural effusion [60]. Some more advanced imaging studies have shown the sensitivity of hyperpolarized ^{13}C-pyruvate MR spectroscopic imaging to metabolic changes (lactate-to-pyruvate signal ratios) associated with lung irradiation and the use of positron emission tomography (PET) imaging to detect increased uptake of ^{18}F-FDG or gallium 68 in areas of inflammation in the lung [62–64]. Yet currently the only current accurate preclinical measurement of damage in the lungs is through extensive biological analysis including breathing rate measurements, bioinformatics methods and by quantifying immune cells using flow cytometry, histology and proteomics [65,66].

In this study, the early inflammatory response of RILI was assessed by serum profiling to map the pro-inflammatory cytokine cascades that drives loss of pulmonary function and lung injury [6,14,32]. Cytokine analysis coupled with gene pathway enrichment and histology was correlated with trends in radiomics features to create novel prediction models of RILI [34,47]. Although C3H mice mainly presented with markers of RP there was a progression to chronic damage with the upregulation of markers of idiopathic pulmonary fibrosis (GDF-15 and CXCL13) at 30 weeks after irradiation [49,67]. In contrast, C57BL6 mice manifested a fibrotic phenotype that was identified as early as 1-week after irradiation from cytokine expression and histology [6]. These data validate C3H mice as a model that presents an early inflammatory phenotype similar to RP and progressively develops to PF at 20/30-weeks after irradiation. Our data also show that C57BL6 are an accurate model of PF from 1-week after irradiation [15,32].

Radiomics can detect RILI's from CT-based scans with recent developments in differentiating healthy or injured lungs [27,68–70]. Studies have shown that CT-based radiomics can significantly outperform traditional dosimetric and clinical predictors for RP alone and combination of these is superior [22,24,26,71,72]. Jiang *et al* showed 11 radiomics features, 5 dosimetric factors, age and T stage to be the best predictors of symptomatic RP [24]. Two of these radiomics features were also identified in our predictive models (first-order range and NGTDM complexity). Qin *et al* identified radiomics features significantly correlated with lung toxicity after stereotactic body RT (SBRT) from longitudinal CBCT scans [73]. Interestingly, the same NGTDM feature was also identified in our study to be correlated with lung injury. Cunliffe *et al* found 12 CT-features which were significant between patients with or without RP [27]. Two of the first-order features were also identified in our models of RP and PF. These studies have demonstrated the advantage of using radiomics analysis to improve prediction models but have yet to longitudinally correlate radiomics features to biological endpoints.

Our study is the first to build predictive models for early inflammatory and late fibrotic phenotypes after lung irradiation using preclinical CBCT radiomics analysis. This is a valid and potentially valuable approach given that current studies rely on monitoring changes in lung

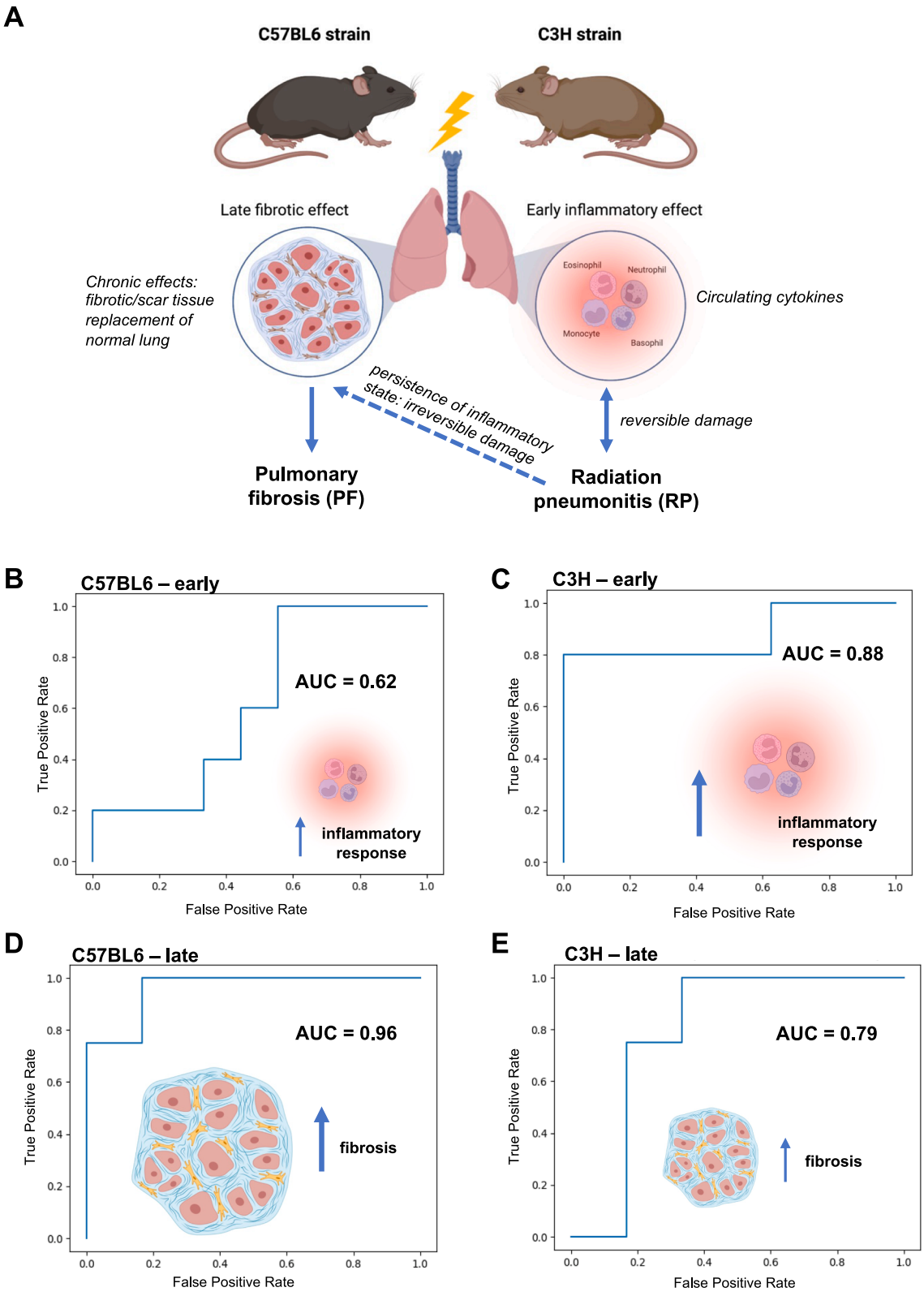

Fig. 5. Deep learning radiomics approach for the prediction of early inflammatory or late fibrotic effects caused by radiation induced lung damage. Panel A: Schematic overview of study to model Radiation-Induced Lung Injury (RILI). C3H mice model early inflammatory effects through the infiltration of immune cells to the affected region. The persistence of this inflammatory state (radiation pneumonitis) can develop to irreversible late toxicity (fibrosis). C57BL6 mice model are highly radiosensitive and model late chronic RILI (pulmonary fibrosis). Panels B-E: For each strain, control and irradiated cohorts were split into training and validation cohorts (70:30) for scans. Scans used for models included for early toxicities included: n = 30 control scans (15 baseline & 15 1-week) and n = 18 irradiated scans (1-week) and for late effects included: n = 25 control scans (15 baseline & 5 20-weeks & 5 30-weeks) and n = 12 irradiated scans (6 20-week & 6 30-week). The receiver operating characteristic (ROC) curves for the random forest models of validation sets for early (Panels B & C) and late (Panels D & E) effects are based on 5 radiomics features identified through recursive feature elimination (RFE).

density, whenever damage is already well established, and retrospective histological analysis to determine the extent of this damage. Density measurements can be very useful for single centre studies for identifying a damaged area of the lung but can be ambiguous in the type of damage, how extensive it is and may not be able comparable with other studies. Encouragingly, some of the quantitative features used to build the predictive models in this study have already been identified in clinical cohorts [27,73]. Two of our models had excellent prediction capabilities of the inflammatory response at 1 week and early detection of fibrosis at 20–30 weeks in C3H mice. However, as expected the model with the highest predictive power was for PF at 20–30 weeks in C57BL6 mice with an AUC of 0.96. Another advantage of our study is that the observed CBCT radiomics features were correlated with circulating and histological biomarkers of RILI at longitudinal imaging timepoints which is not feasible from clinical radiomics studies.

Genetically identical mouse strains provide a homogeneous population for biomarker discovery that is not confounded by genetic variations, patient specific factors (e.g. age, sex, smoking status), comorbidities (e.g. pre-existing cardiovascular diseases) or treatment combinations [14,74]. However, the translation of radiomics features from murine models to clinical imaging was not performed in this study. Furthermore, additional experiments are required to validate these findings with functional endpoints, longer follow-up to refine the signatures and using pooled datasets across multiple centres. Novel tools like spatial transcriptomics could provide additional advanced histological analysis through the molecular and gene profiling from tissue samples. Future preclinical studies would highly benefit from the correlation of spatial transcriptomics outputs with radiomics features, a correlation that can only be developed in these preclinical models [75,76]. Once optimised it will be essential to validate these models in a clinical cohort to identify a predictive biomarker that can help identify patients with RILI. This will enable personalised treatment schedules with changes to radiotherapy dose or therapeutic intervention. Despite the limitations, this study provides promising proof of concept for the development of predictive radiomics signatures and a starting point for future mechanics studies. In first instance, this study shows the benefit of non-invasive imaging to monitoring the burden of RILI and potentially reducing the requirements for large animal numbers during longitudinal sampling studies.

Conclusions

Preclinical CBCT scans are rich datasets that can be interrogated to develop predictive tools for clinically relevant radiotherapy toxicity. In this study, radiomics analysis identified features that could predict early and late RILI in pathology specific models and could have potential value for the translation of imaging biomarkers to the clinic.

Fundings sources

KHB is supported by a Training Fellowship from the National Centre for the Replacement Refinement and Reduction of Animal in Research (NC3Rs, NC/V002295/1). MG and KTB are supported by the Medical Research Council (MR/V009605/1). BNK is supported by the Higher Education Academy North-South Research Funding Programme 2021. LMS is supported by a PhD studentship from Department for the Economy (Northern Ireland).

CRediT authorship contribution statement

Kathryn H. Brown: Conceptualization, Methodology, Formal analysis, Writing – original draft. **Mihaela Ghita-Pettigrew:** Formal analysis, Methodology, Writing – review & editing. **Brianna N. Kerr:** Formal analysis, Methodology, Writing – review & editing. **Letitia Mohamed-Smith:** Methodology. **Gerard M. Walls:** Conceptualization, Methodology, Writing – review & editing. **Conor K. McGarry:** Conceptualization, Methodology, Supervision, Writing – review & editing. **Karl T. Butterworth:** Conceptualization, Supervision, Writing – review & editing.

Declaration of competing interest

The authors declare that they have no known competing financial interests or personal relationships that could have appeared to influence the work reported in this paper.

Appendix A. Supplementary material

Supplementary data to this article can be found online at https://doi.org/10.1016/j.radonc.2024.110106.

References

[1] Faivre-Finn C, et al. Concurrent once-daily versus twice-daily chemoradiotherapy in patients with limited-stage small-cell lung cancer (CONVERT): an open-label, phase 3, randomised, superiority trial. Lancet Oncol 2017;18:1116–25.
[2] Spigel DR, et al. Five-year survival outcomes from the PACIFIC trial: Durvalumab after chemoradiotherapy in stage III non-small-cell lung cancer. J Clin Oncol 2022; 40:1301–11.
[3] Ghita M, et al. Preclinical models of radiation-induced lung damage: challenges and opportunities for small animal radiotherapy. Br J Radiol 2019;92.
[4] Williams JP, Newhauser W. Normal tissue damage: its importance, history and challenges for the future. Br J Radiol 2019;92.
[5] Graves PR, Siddiqui F, Anscher MS, Movsas B. Radiation pulmonary toxicity: From mechanisms to management. Semin Radiat Oncol 2010;20:201–7.
[6] Liu, X., Shao, C. & Fu, J. Promising biomarkers of radiation-induced lung injury: A review. *Biomedicines* vol. 9 Preprint at https://doi.org/10.3390/biomedicines9091181 (2021).
[7] Baker S, Dahele M, Lagerwaard FJ, Senan S. A critical review of recent developments in radiotherapy for non-small cell lung cancer. Radiat Oncol 2016; 11.
[8] Wang J-Y, et al. Outcome and prognostic factors for patients with non-small-cell lung cancer and severe radiation pneumonitis. Int J Radiation Oncology Biol Phys 2002;54:735–41.
[9] Palma DA, et al. Predicting radiation pneumonitis after chemoradiation therapy for lung cancer: An international individual patient data meta-analysis. Int J Radiat Oncol Biol Phys 2013;85:444–50.
[10] Moldoveanu B, et al. Inflammatory mechanisms in the lung. J Inflamm Res 2009;2: 1–11.
[11] Mehta V. Radiation pneumonitis and pulmonary fibrosis in non-small-cell lung cancer: Pulmonary function, prediction, and prevention. Int J Radiat Oncol Biol Phys 2005;63:5–24.
[12] Hanania, A. N., Mainwaring, W., Ghebre, Y. T., Hanania, N. A. & Ludwig, M. Radiation-Induced Lung Injury: Assessment and Management. *Chest* vol. 156 150–162 Preprint at https://doi.org/10.1016/j.chest.2019.03.033 (2019).
[13] Abratt RP, Morgan GW. Lung toxicity following chest irradiation in patients with lung cancer. Lung Cancer 2002;35:103–9.
[14] Giuranno, L., Ient, J., De Ruysscher, D. & Vooijs, M. A. Radiation-Induced Lung Injury (RILI). *Frontiers in Oncology* vol. 9 Preprint at https://doi.org/10.3389/fonc.2019.00877 (2019).
[15] Arroyo-Hernández, M. *et al.* Radiation-induced lung injury: current evidence. *BMC Pulmonary Medicine* vol. 21 Preprint at https://doi.org/10.1186/s12890-020-01376-4 (2021).
[16] Diot Q, et al. Regional normal lung tissue density changes in patients treated with stereotactic body radiation therapy for lung tumors. Int J Radiat Oncol Biol Phys 2012;84:1024–30.
[17] Defraene G, et al. Radiation-Induced Lung Density Changes on CT Scan for NSCLC: No Impact of Dose-Escalation Level or Volume. Int J Radiat Oncol Biol Phys 2018; 102:642–50.
[18] Szmul A, et al. A novel and automated approach to classify radiation induced lung tissue damage on CT scans. Cancers (Basel) 2022;14.
[19] R.S. Kirkland et al. Predictors of In-Hospital Death in Patients with Lung Cancer Admitted for Acute Radiation Pneumonitis: A Healthcare Cost and Utilization Project (HCUP) Analysis Clin Lung Cancer 22 2021 e716 e722.
[20] Inoue, A. *et al. Radiation Pneumonitis in Lung Cancer Patients: A Retrospective Study of Risk Factors and the Long-term Prognosis.* (2001).
[21] Kong, F. M. (Spring) & Wang, S. Nondosimetric Risk Factors for Radiation-Induced Lung Toxicity. *Seminars in Radiation Oncology* vol. 25 100–109 Preprint at https://doi.org/10.1016/j.semradonc.2014.12.003 (2015).
[22] Krafft SP, et al. The utility of quantitative CT radiomics features for improved prediction of radiation pneumonitis. Med Phys 2018;45:5317–24.
[23] Luo Y, et al. A multiobjective Bayesian networks approach for joint prediction of tumor local control and radiation pneumonitis in nonsmall-cell lung cancer (NSCLC) for response-adapted radiotherapy. Med Phys 2018;45:3980–95.
[24] Jiang W, Song Y, Sun Z, Qiu J, Shi L. Dosimetric factors and radiomics features within different regions of interest in planning CT images for improving the prediction of radiation pneumonitis. Int J Radiat Oncol Biol Phys 2021;110: 1161–70.

[25] Aerts HJWL, et al. Decoding tumour phenotype by noninvasive imaging using a quantitative radiomics approach. Nat Commun 2014;5.
[26] Thomas HMT, et al. Radiation and immune checkpoint inhibitor-mediated pneumonitis risk stratification in patients with locally advanced non-small cell lung cancer: role of functional lung radiomics? Discover Oncol 2022;13.
[27] Cunliffe A, et al. Lung texture in serial thoracic computed tomography scans: Correlation of radiomics-based features with radiation therapy dose and radiation pneumonitis development. Int J Radiat Oncol Biol Phys 2015;91:1048–56.
[28] Walls GM, et al. Radiomics for predicting lung cancer outcomes following radiotherapy: A systematic review. Clin Oncol 2021. https://doi.org/10.1016/j.clon.2021.10.006.
[29] Butterworth KT. Evolution of the supermodel: Progress in modelling radiotherapy response in mice. Clin Oncol (R Coll Radiol) 2019;31:272–82.
[30] Brown KH, et al. A scoping review of small animal image-guided radiotherapy research: Advances, impact and future opportunities in translational radiobiology. Clin Transl Radiat Oncol 2022;34:112–9.
[31] Ao X, et al. Radiation produces differential changes in cytokine profiles in radiation lung fibrosis sensitive and resistant mice. J Hematol Oncol 2009;2.
[32] Wirsdörfer, F. & Jendrossek, V. The role of lymphocytes in radiotherapy-induced adverse late effects in the lung. *Frontiers in Immunology* vol. 7 Preprint at https://doi.org/10.3389/fimmu.2016.00591 (2016).
[33] Paun A, Kunwar A, Haston CK. Acute adaptive immune response correlates with late radiation-induced pulmonary fibrosis in mice. Radiat Oncol 2015;10.
[34] Ghita M, et al. Preclinical evaluation of dose-volume effects and lung toxicity occurring in and out-of-field. Int J Radiat Oncol Biol Phys 2019;103:1231–40.
[35] Curras-Alonso S, et al. An interactive murine single-cell atlas of the lung responses to radiation injury. Nat Commun 2023;14.
[36] Dabjan, M. B. *et al.* A survey of changing trends in modelling radiation lung injury in mice: Bringing out the good, the bad, and the uncertain. *Laboratory Investigation* vol. 96 936–949 Preprint at https://doi.org/10.1038/labinvest.2016.76 (2016).
[37] McGrath, J. C. & Lilley, E. Implementing guidelines on reporting research using animals (ARRIVE etc.): New requirements for publication in BJP. *Br J Pharmacol* **172**, 3189–3193 (2015).
[38] Rosser, K. E. The IPEMB code of practice for the determination of absorbed dose for x-rays below 300 kV generating potential (0.035 mm Al-4 mm Cu HVL; 10-300 kV generating potential). Institution of Physics and Engineering in Medicine and Biology. *Phys Med Biol* **41**, 2605–2625 (1996).
[39] Chen, E. Y. *et al. Enrichr: interactive and collaborative HTML5 gene list enrichment analysis tool.* http://amp.pharm.mssm.edu/Enrichr. (2013).
[40] Brown KH, et al. Assessment of variabilities in lung-contouring methods on CBCT preclinical radiomics outputs. Cancers (Basel) 2023;15:2677.
[41] Van Griethuysen JJM, et al. Computational radiomics system to decode the radiographic phenotype. Cancer Res 2017;77:e104–7.
[42] Brown KH, et al. Development and optimisation of a preclinical cone beam computed tomography-based radiomics workflow for radiation oncology research. Phys Imaging Radiat Oncol 2023;26.
[43] Zwanenburg, A., Leger, S., Vallières, M. & Löck, S. Image biomarker standardisation initiative. (2016) doi:10.1148/radiol.2020191145.
[44] Lavrova E, et al. Precision-medicine-toolbox: An open-source python package for the quantitative medical image analysis[Formula presented]. Software Impacts 2023;16.
[45] Hua J, Xiong Z, Lowey J, Suh E, Dougherty ER. Optimal number of features as a function of sample size for various classification rules. Bioinformatics 2005;21:1509–15.
[46] Li, Y. *et al.* The Role of IL-6 in Fibrotic Diseases: Molecular and Cellular Mechanisms. *International Journal of Biological Sciences* vol. 18 5405–5414 Preprint at https://doi.org/10.7150/ijbs.75876 (2022).
[47] She, Y. X., Yu, Q. Y. & Tang, X. X. Role of interleukins in the pathogenesis of pulmonary fibrosis. *Cell Death Discovery* vol. 7 Preprint at https://doi.org/10.1038/s41420-021-00437-9 (2021).
[48] Anas, A., Van Der Poll, T. & De Vos, A. F. Role of CD14 in Lung Inflammation and Infection. *Intensive Care Med* 129–140 (2011) doi:10.1007/978-1-4419-5562-3_13.
[49] Vuga LJ, et al. C-X-C motif chemokine 13 (CXCL13) is a prognostic biomarker of idiopathic pulmonary fibrosis. Am J Respir Crit Care Med 2014;189:966–74.
[50] Clarke E, Curtis J, Brada M. Incidence and evolution of imaging changes on cone-beam CT during and after radical radiotherapy for non-small cell lung cancer. Radiother Oncol 2019;132:121–6.
[51] Walls GM, et al. Clinico-radiological outcomes after radical radiotherapy for lung cancer in patients with interstitial lung disease. *BJR*|Open 2023. https://doi.org/10.1259/bjro.20220049.
[52] Phernambucq ECJ, Palma DA, Vincent A, Smit EF, Senan S. Time and dose-related changes in radiological lung density after concurrent chemoradiotherapy for lung cancer. Lung Cancer 2011;74:451–6.
[53] Schröder C, Engenhart-Cabillic R, Kirschner S, Blank E, Buchali A. Changes of lung parenchyma density following high dose radiation therapy for thoracic carcinomas - An automated analysis of follow up CT scans. Radiat Oncol 2019;14.
[54] Al-Umairi R, et al. CT patterns and serial CT Changes in lung Cancer patients post stereotactic body radiotherapy (SBRT). Cancer Imaging 2022;22.
[55] National Cancer Institute. Common Terminology Criteria for Adverse Events v3.0 (CTCAE). https://ctep.cancer.gov/protocoldevelopment/electronic_applications/docs/ctcaev3.pdf (2006).
[56] Jackson IL, Vujaskovic Z, Down JD. Revisiting strain-related differences in radiation sensitivity of the mouse lung: Recognizing and avoiding the confounding effects of pleural effusions. Radiat Res 2010;173:10–20.
[57] Dunne V, et al. Inhibition of ataxia telangiectasia related-3 (ATR) improves therapeutic index in preclinical models of non-small cell lung cancer (NSCLC) radiotherapy. Radiother Oncol 2017;124:475–81.
[58] Spiegelberg L, et al. Evofosfamide sensitizes esophageal carcinomas to radiation without increasing normal tissue toxicity. Radiother Oncol 2019;141:247–55.
[59] van Berlo D, et al. Micro cone beam computed tomography for sensitive assessment of radiation-induced late lung toxicity in preclinical models. Radiother Oncol 2019;138:17–24.
[60] Saito S, Murase K. Detection and early phase assessment of radiation-induced lung injury in mice using micro-CT. PLoS One 2012;7.
[61] Meyerholz, D. K., Sieren, J. C., Beck, A. P. & Flaherty, H. A. Approaches to Evaluate Lung Inflammation in Translational Research. *Veterinary Pathology* vol. 55 42–52 Preprint at https://doi.org/10.1177/0300985817726117 (2018).
[62] Abravan A, et al. A new method to assess pulmonary changes using 18F-fluoro-2-deoxyglucose positron emission tomography for lung cancer patients following radiotherapy. Acta Oncol (Madr) 2017;56:1597–603.
[63] Thind K, et al. Detection of radiation-induced lung injury using hyperpolarized 13C magnetic resonance spectroscopy and imaging. Magn Reson Med 2013;70:601–9.
[64] Lucia F, et al. Prediction of acute radiation-induced lung toxicity after stereotactic body radiation therapy using dose-volume parameters from functional mapping on gallium 68 perfusion positron emission tomography/computed tomography. Int J Radiat Oncol Biol Phys 2023. https://doi.org/10.1016/j.ijrobp.2023.10.004.
[65] Groves AM, et al. Influence of the irradiated pulmonary microenvironment on macrophage and T cell dynamics. Radiother Oncol 2023;183.
[66] El Naqa I, Spencer SJ, Almiron Bonnin D, Deasy JO, Bradley JD. Bioinformatics methods for learning radiation-induced lung inflammation from heterogeneous retrospective and prospective data. J Biomed Biotechnol 2009;2009.
[67] Radwanska A, et al. Increased expression and accumulation of GDF15 in IPF extracellular matrix contribute to fibrosis. Ref Inform: JCI Insight 2022;7.
[68] Anthony GJ, et al. Incorporation of pre-therapy 18F-FDG uptake data with CT texture features into a radiomics model for radiation pneumonitis diagnosis. Med Phys 2017;44:3686–94.
[69] Hoffman EA, et al. Characterization of the interstitial lung diseases via density-based and texture-based analysis of computed tomography images of lung structure and function1. Acad Radiol 2003;10:1104–18.
[70] Chabat F, Yang G-Z, Hansell DM. Obstructive lung diseases: Texture classification for differentiation at CT. Radiology 2003;228:871–7.
[71] Bousabarah K, et al. Radiomics for prediction of radiation-induced lung injury and oncologic outcome after robotic stereotactic body radiotherapy of lung cancer: results from two independent institutions. Radiat Oncol 2021;16.
[72] Wang L, et al. Computed tomography-based delta-radiomics analysis for discriminating radiation pneumonitis in patients with esophageal cancer after radiation therapy. Int J Radiat Oncol Biol Phys 2021;111:443–55.
[73] Qin Q, et al. Cone-beam CT radiomics features might improve the prediction of lung toxicity after SBRT in stage I NSCLC patients. Thorac Cancer 2020;11:964–72.
[74] Leduc C, Antoni D, Charloux A, Falcoz PE, Quoix E. Comorbidities in the management of patients with lung cancer. Eur Respir J 2017;49.
[75] Walls GM, et al. Spatial gene expression changes in the mouse heart after base-targeted irradiation. Int J Radiat Oncol Biol Phys 2023;115:453–63.
[76] Marx V. Method of the Year: spatially resolved transcriptomics. Nat Methods 2021;18:9–14.